arXiv:1612.07211v1 [cond-mat.str-el] 21 Dec 2016

Three-dimensional critical phase diagram of the Ising antiferromagnet $CeRh_2Si_2$ under intense magnetic field and pressure

W. Knafo,[1] R. Settai,[2] D. Braithwaite,[3] S. Kurahashi,[4] D. Aoki,[3,5] and J. Flouquet[3]

[1] *Laboratoire National des Champs Magnétiques Intenses, UPR 3228, CNRS-UPS-INSA-UGA, 143 Avenue de Rangueil, 31400 Toulouse, France*
[2] *Department of Physics, Faculty of Science, Niigata University, 8050 Ninocho Ikarashi, Nishi-ku, Niigata 950-2181, Japan*
[3] *Université Grenoble Alpes and CEA, INAC-PHELIQS, F-38000 Grenoble, France*
[4] *Graduate School of Science and Technology, Niigata University, 8050 Ninocho Ikarashi, Nishi-ku, Niigata 950-2181, Japan*
[5] *Institute for Materials Research, Tohoku University, Ibaraki 311-1313, Japan*

(Dated: December 22, 2016)

Using novel instrumentation to combine extreme conditions of intense pulsed magnetic field up to 60 T and high pressure up to 4 GPa, we have established the three-dimensional (3D) magnetic field - pressure - temperature phase diagram of a pure stoichiometric heavy-fermion antiferromagnet ($CeRh_2Si_2$). We find a temperature- and pressure-dependent decoupling of the critical and pseudo-metamagnetic fields, at the borderlines of antiferromagnetism and strongly-correlated paramagnetism. This 3D phase diagram is representative of a class of heavy-fermion Ising antiferromagnets, where long-range magnetic ordering is decoupled from a maximum in the magnetic susceptibility. The combination of extreme conditions enabled us to characterize different quantum phase transitions, where peculiar quantum critical properties are revealed. The interest to couple the effects of magnetic field and pressure on quantum-critical correlated-electron systems is stressed.

PACS numbers: 71.27.+a,74.70.Tx,75.30.Kz,75.30.Mb

I. INTRODUCTION

The importance of quantum criticality [1] has been emphasized for a large variety of electronic materials, ranging from high-temperature - cuprate [2] and iron-based [3] - superconductors, heavy-fermion systems [4], to low-dimensional quantum magnets [5, 6], tuned by chemical doping, high pressure, or intense magnetic field. In many of these systems both pressure (or doping) and magnetic field can destabilize a magnetically-ordered phase and lead to critical non-Fermi liquid behaviors [7, 8]. However, the critical properties they induce are not necessarily equivalent. While pressure usually drives to a quantum phase transition between a magnetically-ordered state and a paramagnetic (PM) regime, a magnetic field leads to drastically-different effects caused by the polarization of the magnetic moments along the field direction. The comparison between the effects of magnetic field and pressure on quantum criticality has been scarcely explored so far, mainly due to the experimental challenges of such experiments under combined extreme conditions, to which one should add a third dimension, the temperature. For this purpose, heavy-fermion materials are ideal systems: they present the unique advantage of having low electronic energy scales, which allows their quantum critical properties to be tuned by experimentally-accessible pressures and fields. From now on we will focus on Ce-based anisotropic heavy-fermion antiferromagnets, to which belongs $CeRh_2Si_2$ investigated here. In the following, we present the main features of their 3D magnetic phase diagram, drawn schematically in Fig. 1.

Applied to Ce-based antiferromagnets, pressure can tune the electronic correlations and induce a quantum magnetic phase transition at a critical pressure p_c, where the antiferromagnetic (AF) ordering temperature T_N collapses to zero and is replaced by a correlated paramagnetic (CPM) regime. Well-defined anomalies (for instance steps or kinks in the magnetic susceptibility χ, the heat capacity C_p, and the electrical resistivity ρ) are the signature of the phase transitions at T_N and p_c. The onset of the CPM regime is a crossover and consists in a progressive change of the physical properties induced by low-temperature electronic correlations. Strong inter-site magnetic fluctuations are generally observed in the CPM regime of anisotropic heavy-fermion paramagnets, indicating the proximity of quantum magnetic instabilities [9]. Several characteristic temperatures (instead of a unique critical temperature at a phase transition) can be associated with this crossover to the CPM regime. Its setting in leads to a broad maximum of χ at the temperature T_χ^{max}, below which χ almost saturates [9, 10]. At low temperature, the relation $\chi \propto \gamma \propto m^*$, where γ is the Sommerfeld coefficient $\gamma = C_p/T$ and C_p is the specific heat, is verified, indicating a Fermi liquid behavior associated with an effective mass m^* [11]. The crossover to the CPM regime also leads to a broad maximum at the temperature T_ρ^{max} in the electronic (non-phononic) contribution ρ^{el} to the electrical resistivity, which is related with an inflexion point at a temperature $T_{\partial\rho/\partial H}^{max} < T_\rho^{max}$ in the resistivity [12]. A similarity between the broad anomalies observed at T_χ^{max} in χ and at T_ρ^{max} in ρ^{el} has been emphasized [13]. A T^2 Fermi-liquid variation of the resistivity, with a quadratic coefficient $A \propto m^{*2}$, is also generally observed at tem-

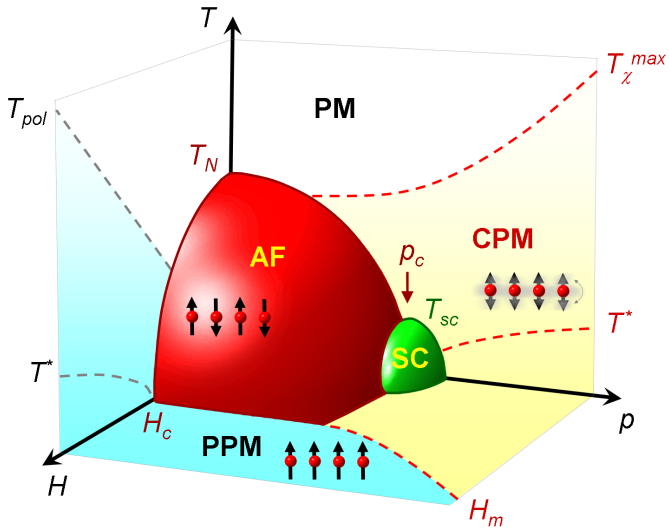

FIG. 1. Schematic magnetic field - pressure - temperature phase diagram of heavy-fermion antiferromagnets. AF, SC, CPM and PPM denote the antiferromagnetic and superconducting phases, the correlated paramagnetic and polarized paramagnetic regimes, respectively. Sketches of antiferromagnetic moments, polarized moments, and fluctuating moments (assuming Ising magnetic anisotropy) are presented for the AF phase and the PPM and CPM regimes, respectively. All parameters T_N, T_χ^{max}, T_{pol}, T_{sc}, p_c, H_c, and H_m presented in this phase diagram have been defined in Section I.

peratures below T^* [14]. These different temperature scales, with a hierarchy $T^* \ll T_{\partial\rho/\partial H}^{max} < T_\rho^{max}, T_\chi^{max}$ generally observed in heavy-fermion paramagnets (cf. the prototypical heavy-fermion paramagnet $CeRu_2Si_2$, where $T^* \simeq 500$ mK [15] and $T_\chi^{max} \simeq 10$ K [16]), are all linked to the crossover into the CPM regime. Fermi-liquid behavior is not restricted to the CPM regime and can be observed inside the antiferromagnetic state. At p_c, T^* passes through a minimum or vanishes, whereas the resistivity coefficient A is maximal and may even show a divergence [17]. Driven by quantum criticality, i.e., usually by critical magnetic fluctuations, heavy effective masses m^* can reach up to a thousand times that of the free electrons [18, 19]. In many systems, low-temperature superconductivity mediated by the critical magnetic fluctuations also develops below a temperature T_{sc} in the vicinity of p_c [20]. Interestingly, in several heavy-fermion antiferromagnets, a broad maximum of susceptibility is observed at a temperature T_χ^{max} higher than the Néel temperature T_N, indicating a CPM regime preceding the AF ordering [9, 10] (see Fig. 1 at pressures just below p_c).

Quantum criticality can also be reached by applying magnetic field, which destroys magnetic order and leads to a quantum phase transition to a polarized paramagnet (PPM) regime, above which a large part of the magnetic moments is aligned, at a critical field H_c [9, 21]. In strongly-anisotropic heavy-fermion antiferromagnets, H_c varies significantly with the field-direction and spin-flop transitions [22] are forbidden. This contrasts with the case of isotropic or nearly-isotropic antiferromagnets, where H_c is almost-independent of the field direction and where spin-flop transitions [23] (or crossovers controlled by a spin-flop-like domain alignment [24]) can be induced at low field. When the Ising anisotropy is strong, a magnetic field applied along the easy axis induces a first-order metamagnetic transition at H_c. Well-defined anomalies are induced at the transition field H_c in measured physical quantities, such as a jump in the magnetization driven by a sudden polarization of the moments along the field direction [25, 26], or a sudden step in ρ at low temperature, which is replaced by kink when the temperature is raised [27]. Similarly to the pressure effect, an enhancement of the resistivity coefficient A and a vanishing of T^* have been reported at H_c [17]. In anisotropic heavy-fermion paramagnets, a magnetic field applied along the easy axis also leads to a PPM regime, at a pseudo-metamagnetic field usually noted H_m [9, 28]. H_m corresponds to a magnetic crossover and leads to broad anomalies in measured physical quantities, as a rounded step in ρ at low-temperature, which transforms into a broad maximum when the temperature is raised [15]. Although they are both paramagnetic, the low-temperature CPM and PPM regimes may differ significantly. The CPM regime is characterized by strong electronic correlations and a small magnetic polarization under magnetic field, while the PPM regime is associated with a strong magnetic polarization and reduced intersite electronic correlations. This difference is highlighted in the prototypical heavy-fermion paramagnet $CeRu_2Si_2$, where antiferromagnetic fluctuations are present in the CPM state but vanish in the PPM regime [29, 30]. Under high fields, a high-temperature scale T_{pol} also indicates the crossover from the low-temperature PPM regime to the high-temperature paramagnetic regime, being associated with a progressive loss of the field-induced magnetic polarization when the temperature is raised.

In the Ising antiferromagnet $CeRh_2Si_2$ investigated here, the Néel temperature T_N of 36 K at ambient pressure, below which AF moments are aligned along **c** [31], vanishes under a pressure $p_c \simeq 1$ GPa [32, 33]. Superconductivity appears in a restricted pressure window around p_c [34, 35]. A magnetic field $\mu_0 H_c = 26$ T applied along **c** induces a first-order transition into the PPM regime [26, 27, 36], which is pushed to higher fields under pressure [37]. Pressure- and magnetic-field-induced changes of the magnetic structure inside the AF phase have also been reported [27, 32, 35]. Contrary to most other Ce-systems where a non-Fermi-liquid behavior is found, a low-temperature Fermi-liquid T^2 dependence of the resistivity is reported in $CeRh_2Si_2$ at all pressures and magnetic fields [27, 35], including at p_c and H_c where first-order transitions occur. Although the superconducting (SC), PM and/or AF phases boundaries have been determined for several compounds in restricted pressure, field, and temperature windows [9, 21, 38–40], a full (H,p,T)

phase diagram, including the temperature and pressure evolution of the critical lines H_c and H_m, had not been established yet for a pure stoichiometric compound.

Here, we explore the complete three-dimensional (H,p,T) phase diagram of $CeRh_2Si_2$, and we extract its magnetic-field- and pressure-induced quantum critical properties. In particular, the need to consider carefully the high-temperature properties to understand the complex quantum critical properties in the (H,p) plane, i.e., at the borderlines between the AF, CPM, and PPM quantum states, is emphasized. After an introduction to the experimental techniques in Section II, magnetoresistivity data and the 3D magnetic phase diagram obtained here are presented in Section III. A comparison of the temperature and magnetic field scales, and an extraction of the quantum critical properties (via the quadratic coefficient A in the resistivity), are presented in Section IV. Finally, discussion and conclusion are made in Sections V and VI, respectively.

II. EXPERIMENTAL TECHNIQUES

The single crystals studied here were grown by the Czochralsky method in a tetra-arc furnace. Magnetoresistivity measurements have been performed under combined extreme conditions of high pressure up to 4 GPa, pulsed magnetic fields up to 60 T, and temperatures down to 1.4 K. The results presented here correspond to four sets of experiments under pulsed magnetic fields (using four single crystals: samples ♯1, ♯2, ♯3, and ♯4): the first one at ambient pressure (cf. [27] for the experiment details), and the three others using a pressure cell. Residual resistivity ratios $\rho_{x,x}(T = 300\text{K})/\rho_{x,x}(T \to 0)$ of $\simeq$ 50, 40, 145, and 25 were found for samples ♯1, ♯2, ♯3, and ♯4, respectively, at ambient pressure. Two new Bridgman-type pressure cells specially designed - at the Niigata University (cell "1") and the CEA Grenoble (cell "2") - for the pulsed fields have been used in 20-mm bore ^{4}He cryostats under long-duration (rise of 50 ms and fall of 330 ms) pulsed magnetic fields up to 60 T generated at the LNCMI-Toulouse. The electrical resistivity was measured by the four-point technique, at frequencies from 20 to 70 kHz, with a current of 10 mA. Data have been analyzed using digital lock-ins (developed at the LNCMI-T by Hanappel and Fabrèges). Cell "1" was used for a set of measurements on sample ♯2, at the pressures $p = 0.65$, 0.75, 1, 1.2, 1.5, 2, 2.5 and 3 GPa, and cell "2" was used to study sample ♯3 at the pressures $p = 0.95$, 2, 3, and 4 GPa, and sample ♯4 at the pressures $p = 0.65$, 0.75, 0.85, and 0.9 GPa. The pressure was estimated by checking the superconducting transition from the resistivity of a lead sample, placed into the cell close to the $CeRh_2Si_2$ sample, and by comparing the temperature dependence of $\rho_{x,x}$ measured here with data from [12, 41]. To perform experiments under pulsed magnetic fields combined with pressures as high as 4 GPa, the price to pay was to accept small heating effects induced on the sample by the metallic body of the cell, whose other parts (anvils, gasket, etc.) are non-metallic, during the pulsed-field shots. The presented data were recorded during the rise of the field pulses, where the sample heating remains acceptable. Assuming a linear increase of the temperature versus time during the pulse, the temperature of the sample has been corrected to extract the A coefficient and the magnetic phase diagram from the resistivity data. Details about the pressure cells, but also the procedure to estimate the heating effects and correct the sample temperature during the field pulses, can be found in Refs. [42, 43].

III. MAGNETORESISTIVITY AND MAGNETIC PHASE DIAGRAM

The in-plane magnetoresistivity $\rho_{x,x}$ of $CeRh_2Si_2$ under magnetic fields up to 60 T is shown in Fig. 2 for a wide range of pressures and temperatures (cf. [27] for a similar study at ambient pressure). In spite of different residual resistivity ratios varying from 25 to 145, the magnetoresistivity of the four samples investigated here shows similar features, indicating their magnetic - but not orbital - origin (see Ref. [44] and Appendix). For $p < p_c$ (Figs. 2(a-b), $p = 0.65$ and 0.75 GPa) and at low temperature, a step in $\rho_{x,x}$ vs H is seen at the AF borderline H_c, which coincides with H_m. At intermediate temperatures, a decoupling of H_c (kink) and H_m (broad maximum) is seen for $T > T_x = 20$ and 10 K, at $p = 0.65$ and 0.75 GPa, respectively. The maximum of $\rho_{x,x}$, which is ascribed to the pseudo-metamagnetic field H_m, survives above T_N at pressures $p < p_c \simeq 1$ GPa and can be observed down to the lowest temperatures at pressures $p_c \leq p \leq 1.2$ GPa (see Figs. 2(c-d)). At low pressures $p \ll p_c$, the decoupling of H_c and H_m can be observed only in a narrow temperature range $T_x \leq T \leq T_N$, and it is active down to the lowest temperature for pressures just below p_c, as shown in Fig. 3 for the pressures $p = 0.85$ and 0.9 GPa. Conversely to T_N, $\mu_0 H_c$ increases under pressure, from 26 T at $p = 1$ bar to 35 T at $p = 0.75$ GPa. For $p \gtrsim p_c$, H_m at low temperatures is found to increase, reaching 51.5 T at $p = 1.2$ GPa (see Fig. 2(d)). H_m decreases with increasing temperature and we lose its trace at temperatures higher than 50 and 80 K, at the pressures $p = 0.75$ and 1.2 GPa, respectively. At high temperature, another broad maximum in $\rho_{x,x}$ is observed at the field H_{pol}, which increases with increasing T. H_{pol}, which is equivalent to T_{pol} in Fig. 1, is a signature of the crossover between the low-field high-temperature PM and the high-field PPM regimes. At $p = 1.5$ GPa and low temperature, H_m is beyond the experimental window [0;60 T], and we can only see its trace, as well as that of H_{pol}, at temperatures above 65 K (see Fig. 2(e)). At $p = 4$ GPa, no trace of H_m nor H_{pol} can be found up to 141 K, due to field scales far beyond the accessible experimental window (see Fig. 2(f)).

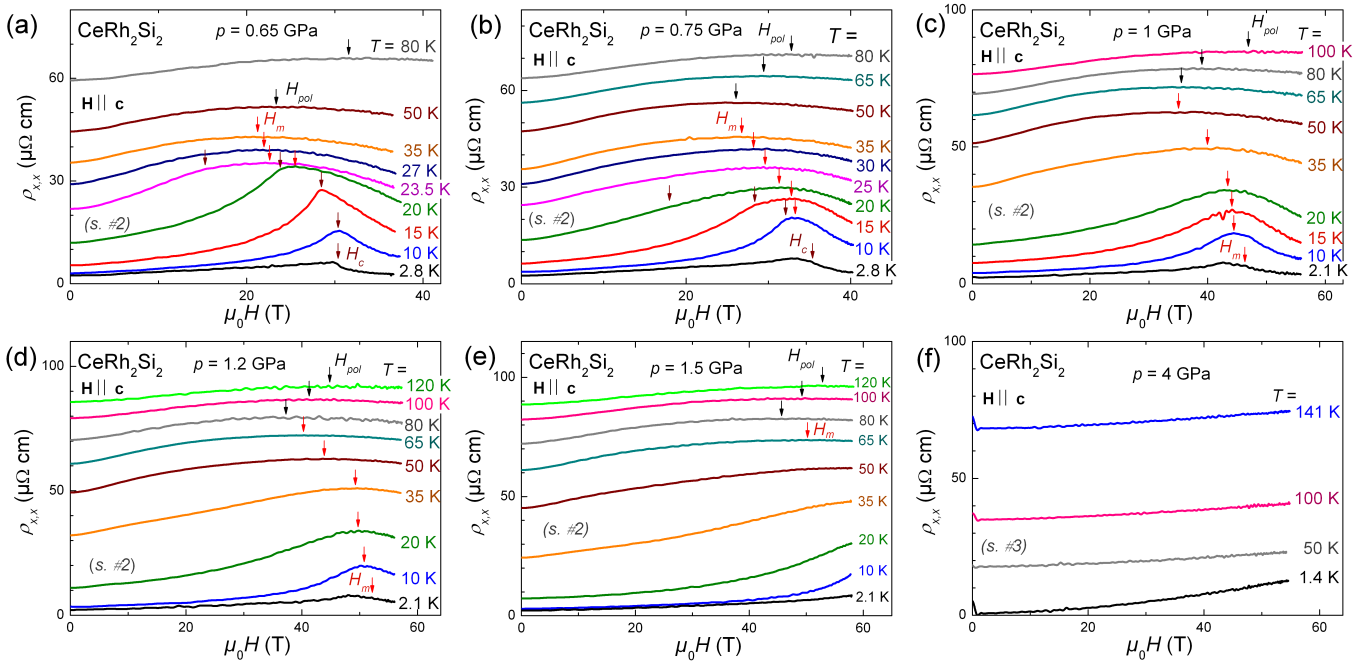

FIG. 2. $\rho_{x,x}$ of $CeRh_2Si_2$ under pressures combined with fields up to 60 T applied along **c** and temperatures $1.4 \leq T \leq 141$ K. Data are presented at (a) $p = 0.65$ GPa (sample ♯2), (b) $p = 0.75$ GPa (sample ♯2), (c) $p = 1$ GPa (sample ♯2), (d) $p = 1.2$ GPa (sample ♯2), (e) $p = 1.5$ GPa (sample ♯2), and(e) $p = 4$ GPa (sample ♯3).

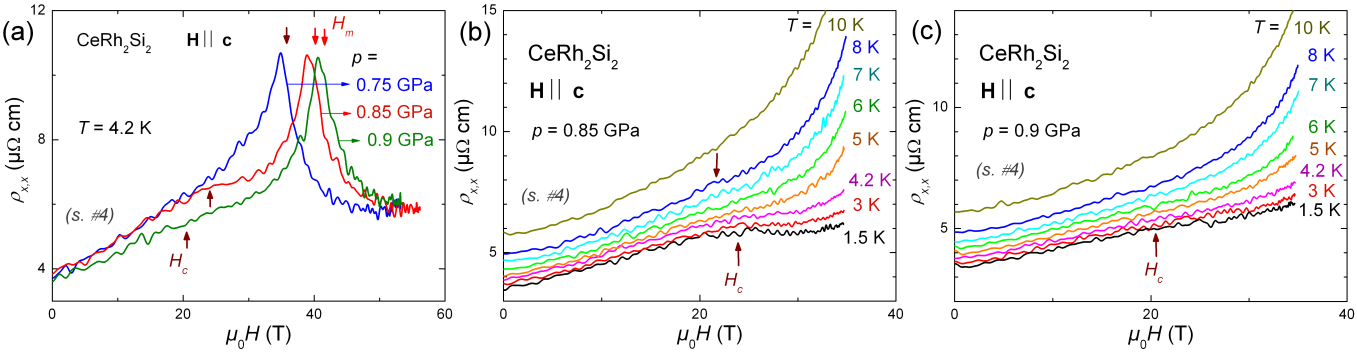

FIG. 3. Magnetic-field-dependence of the resistivity $\rho_{x,x}$ of $CeRh_2Si_2$ emphasizing the low-temperature decoupling of H_c and H_m at pressures just below p_c (sample ♯4). $\rho_{x,x}$ versus H (a) at $T = 4.2$ K and $p = 0.75$, 0.85, and 0.9 GPa, and at $1.5 \leq T \leq 10$ K, in fields $\mu_0 H \leq 35$ T: (b) at $p = 0.85$ GPa and (c) at $p = 0.9$ GPa.

Fig. 4(a) presents the zero-field (p,T) phase diagram of $CeRh_2Si_2$ (constructed using susceptibility data from Ref. [33] and resistivity data from Ref. [35]), showing that antiferromagnetism vanishes at $p_c \simeq 1$ GPa, where superconductivity develops at very low temperature. T_χ^{max} is almost constant for $p < 0.8$ GPa and increases almost linearly with p for $p > 0.8$ GPa. Hence the CPM regime, which exists at temperatures $T_N < T \lesssim T_\chi^{max}$, becomes more extended under pressure and is the low-temperature ground state for $p > p_c$. Figs. 4(b-c) show the (H,T) phase diagrams obtained here at $p = 0.75$ and 1.2 GPa. At $p = 0.75$ GPa and at low temperature, antiferromagnetism vanishes at $\mu_0 H_c \simeq 35$ T, above which the system is polarized paramagnetically. At temperatures $T > T_x = 10$ K, H_c and H_m become separated. The temperature of $\simeq 40$ K at which H_m vanishes and H_{pol} appears coincides with the temperature scale T_χ^{max}. At $p = 0.75$ GPa, the CPM regime is, thus, established at temperatures $T_N < T \lesssim T_\chi^{max}$ and magnetic fields up to H_m. At pressures $p \gtrsim p_c$, the ground state is the CPM regime. The temperature at which its boundary H_m falls and H_{pol} appears is also similar to T_χ^{max}. This indicates that the CPM regime can be delimited by the crossover scales T_χ^{max} and H_m, which both increase with increasing pressure. When $T > T_\chi^{max}$, H_{pol} increases linearly with T at all pressures, as observed at $p = 1$ bar [27], and shows little pressure dependence. Fig. 4(d) presents the (p,H) phase diagram extracted in

the limit $T \to 0$, showing that the AF phase boundary H_c slowly increases with p for $p < p_x = 0.75$ GPa, before suddenly decreasing above p_x. The borderline of the zero-resistivity SC state $\mu_0 H_{SC}$, which reaches $\simeq 0.3$ T for $T \to 0$ (data from [35]), is also plotted in Fig. 4(d). The critical point (p_x,H_x), where $\mu_0 H_x = 35$ T, separates the AF phase, the high-pressure CPM regime, and the high-field PPM regime in the limit $T \to 0$. Interestingly, the pseudo-metamagnetic field H_m increases linearly with p in a similar manner to T_χ^{max} for $p > p_x$ (see Figs. 4(a,d)).

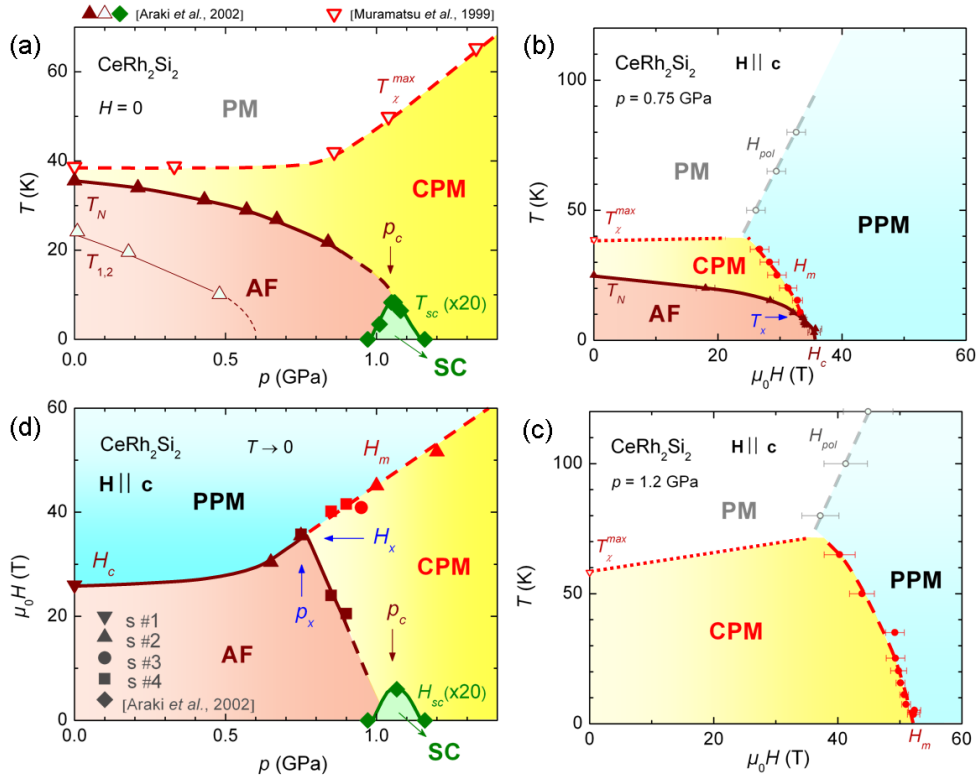

FIG. 4. (H,p,T) phase diagram of $CeRh_2Si_2$ under a magnetic field $\mathbf{H} \parallel \mathbf{c}$. (a) ($p$,$T$) phase diagram at $H = 0$. (b-c) (H,T) phase diagrams at $p = 0.75$ and 1.2 GPa. (d) (p,H) phase diagram in the limit $T \to 0$.

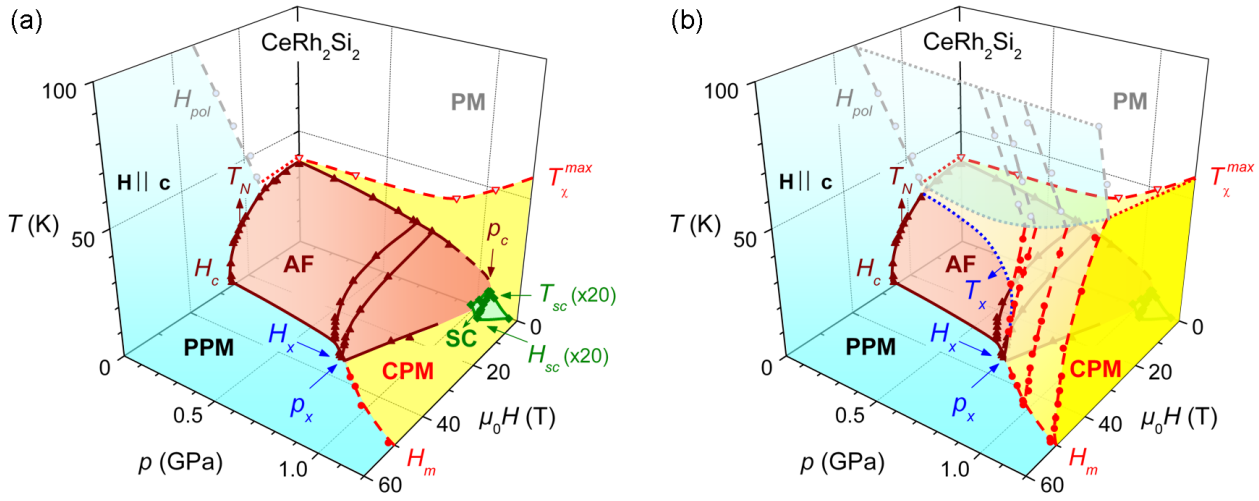

FIG. 5. 3D (H,p,T) phase diagram of $CeRh_2Si_2$ under a magnetic field $\mathbf{H} \parallel \mathbf{c}$, for $\mu_0 H \leq 60$ T, $p \leq 1.2$ GPa, and $1.4 \leq T \leq 100$ K. T_N, $T_{1,2}$, and T_{sc} at zero-field and H_{sc} are reproduced from [35], T_χ^{max} at zero-field is reproduced from [33]. (a) emphasizes the 3D views of the AF and SC phases, while (b) emphasizes the 3D views of the CPM and PPM regimes.

Fig. 5 shows the three-dimensional magnetic field - pressure - temperature phase diagram of $CeRh_2Si_2$ extracted from our magnetoresistivity measurements (but also including data from Refs. [27, 33, 35]). Fig. 5(a) presents a 3D view of the AF and SC phases, while Fig. 5(b) extends the 3D view to the CPM and PPM regimes. These plots permit to show that the CPM regime englobes the AF phase as long as $T > T_x$ at pressures $p < p_c$. Fig. 5(b) emphasizes that the temperature T_x separating the three low-temperature phases decreases under pressure and vanishes at the critical point (H_x,p_x,$T \rightarrow 0$). The decoupling of H_c and H_m and its intimate relationship with the decoupling of T_N and T_χ^{max} are the central features of this phase diagram. We note that the high-temperature border H_{pol} of the PPM regime is almost pressure-independent and defines a high-temperature plane ending on the CPM border.

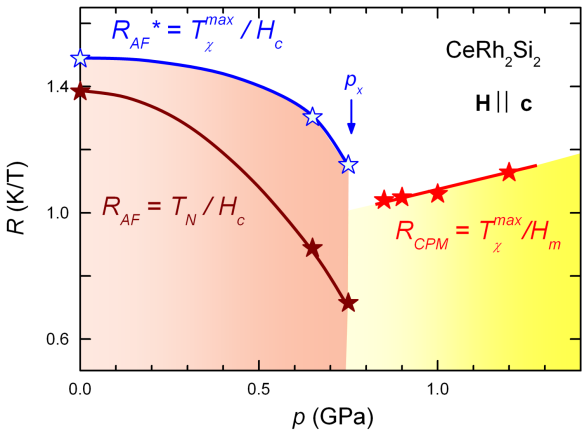

FIG. 6. Pressure dependence of $R_{AF} = T_N/H_c$ and $R^*_{AF} = T_\chi^{max}/H_c$ for $p < p_x$, and $R_{CPM} = T_\chi^{max}/H_m$ for $p > p_x$.

IV. ENERGY SCALES AND QUANTUM CRITICAL PROPERTIES

We can better understand the 3D phase diagram by comparing the pressure dependences of the different energy scales. Fig. 6 shows the pressure dependence of the ratios $R_{CPM} = T_\chi^{max}(H = 0)/H_m(T \rightarrow 0)$ and $R_{AF} = T_N(H = 0)/H_c(T \rightarrow 0)$ extracted for $CeRh_2Si_2$ in its CPM regime and AF phase, respectively. While $R_{CPM} \simeq 1.1$ K/T is almost pressure-independent for $p \geq p_x$, R_{AF} strongly varies with p for $p \leq p_x$. This is consistent with a trend already observed for other heavy-fermion systems [9]. The universal constant $R_{CPM} = T_\chi^{max}/H_m \simeq 1$ K/T characterizes many heavy-fermion paramagnets [9, 45] and indicates that T_χ^{max} and H_m are controlled by a single parameter. In heavy-fermion paramagnets, the magnetic susceptibility almost saturates at temperatures below T_χ^{max} and the low-field magnetization $M(H)$ is linear in fields up to almost H_m. Pseudo-metamagnetism occurs, thus, at a similar critical value of the magnetization ($M_c \simeq 0.5 - 1\ \mu_B$) in heavy-fermions paramagnets where $R_{CPM} \simeq 1$. Conversely, $R_{AF} = T_N/H_c$ is not a universal constant for heavy-fermion antiferromagnets, where multiple parameters have to be considered [9]. As seen in Figs. 4(a,d), the increase of H_c with p for $p \leq p_x$ seems to be linked with that of T_χ^{max}, but not with the decrease with p of T_N. The ratio $R^*_{AF} = T_\chi^{max}(H = 0)/H_c(T \rightarrow 0)$, also plotted in Fig. 6 for $p \leq p_x$, is found to vary less than R_{AF}, showing that H_c is partly controlled by the magnetic interactions which govern T_χ^{max}.

Having established the phase diagram, we now turn to characterize its quantum critical properties by analyzing the evolution of the effective mass, extracted through the temperature dependence of the resistivity, in the two-dimensional quantum plane (H,p). At first approximation, we assume that the quadratic coefficient A in the electrical resistivity $\rho_{x,x} = \rho^0_{x,x} + AT^2$, where $\rho^0_{x,x}$ is the residual resistivity, is proportional to m^{*2}. Here, a T^2 law is observed within the experimental uncertainty in a large temperature window going from 1.5 to $\simeq 8 - 10$ K, for all investigated pressures and magnetic fields. The upper temperature limit of the T^2 law is minimal at the critical fields H_c and H_m and pressure p_c, where it reaches $\simeq 8 - 10$ K, and is maximal in magnetic fields far from H_c and H_m, and pressures far from p_c, where it reaches $\simeq 15$ K (see Appendix). Fig. 7(a) presents the field-dependence of A extracted from $\rho_{x,x}$ versus T curves (reconstructed from $\rho_{x,x}$ versus H data measured at constant temperature; see Appendix) at pressures up to 1.5 GPa. Combined magnetic fields and pressures lead to an enhancement of A at H_c (or H_m) for $p < p_x$ ($p > p_x$). For $p_x < p < p_c$, an enhancement at H_c is not visible in this A versus H plot because the anomaly at H_c is a rather weak and broad shoulder, in comparison with the anomaly at H_m in the $\rho_{x,x}(H)$ measurement. However, the anomaly at H_c is clearly visible as a well-defined maximum in A versus p plots (see Fig. 7(b)) in agreement with the low-temperature (H,p) phase diagram (Fig. 4(d)).

Confirming previous reports [27, 46], the field-driven enhancement of A at ambient pressure is similar to the pressure-driven one at zero-field, the same maximal value of $\simeq 25\ 10^{-3}\ \mu\Omega\text{cmK}^{-2}$ being reached at (H_c, $p = 1$ bar) and ($H = 0$, p_c) (cf. Fig. 11 in the Appendix). However, quite surprisingly, as pressure is increased, the enhancement of A at the field H_c or H_m becomes considerably larger. This is illustrated in Fig. 7(c) by the pressure-dependence of A_{max}, which is defined as the maximal value of A versus H at a given pressure. Quantum criticality at H_c and H_m leads to the maximal values $A_{max} = A(H_c)$ for $p < p_x$ and $A_{max} = A(H_m)$ for $p > p_x$. We remark that the strong increase of A_{max} with p at pressures $p < p_x$ ends in a maximal value of $A_{max} \simeq 150\ 10^{-3}\ \mu\Omega\text{cmK}^{-2}$ at (H_x,p_x), and is followed by an almost pressure-independence of A_{max} for $p \geq p_x$.

V. DISCUSSION

Here, we present the first study of a pure stoichiometric heavy-fermion antiferromagnet, where the decoupling of two critical fields H_c and H_m is systematically investigated as function of temperature and pressure. Such decoupling of H_c and H_m has also been observed down to $T = 100$ mK in the Ising antiferromagnet $Ce(Ru_{0.92}Rh_{0.08})_2Si_2$ at ambient pressure [47], and at $T = 1.8$ K in $Ce_{0.8}La_{0.2}Ru_2Si_2$ under pressure [48]. In the Ising antiferromagnet $Ce_{0.9}La_{0.1}Ru_2Si_2$ at ambient pressure, a decoupling of H_c and H_m has been observed in an intermediate range of temperatures $1.5 \leq T \leq T_N = 4.4$ K [16, 47, 48], but not at temperatures below 1.5 K. While pressure and chemical doping generally lead to similar effects on the magnetic phase diagram of heavy-fermion systems, pressure has the advantage to continuously tune the properties of a single crystal without altering its quality. Its combination with intense magnetic fields over a large temperature window permits here to draw the complete (H,p,T) magnetic phase diagram of $CeRh_2Si_2$. We show that the low-temperature decoupling of H_c and H_m occurs at pressures just below p_c and is connected with a high-temperature phenomenon, the decoupling of T_N and T_χ^{max}. The wrapping of the CPM regime over the AF phase, as seen in the 3D phase diagram in Fig. 5, is a consequence of the decoupling of these magnetic field and temperature scales. The similarities with studies made on Rh- and La-doped $CeRu_2Si_2$ indicate that the complete phase diagram established here for $CeRh_2Si_2$ might be generic of a class of heavy-fermion Ising antiferromagnets, where a decoupling of T_N and T_χ^{max} drives that of H_c and H_m.

However, the quantum critical properties at H_c and H_m are sensitive to specific sample properties. In $CeRh_2Si_2$, the highest value of A is reached on the H_m critical line, where $A = A(H_m)$ is pressure-independent. Oppositely, in La-doped $CeRu_2Si_2$, $A(H_m)$ decreases with p while the Sommerfeld coefficient γ ($\propto \sqrt{A}$ in a Fermi liquid picture) is maximal and constant at H_c [49]. Microscopically, we speculate that the enhancement of A at p_c is controlled by critical antiferromagnetic fluctuations (similarly to the $Ce_{1-x}La_xRu_2Si_2$ case [4]), while that found at H_m may result from additional mechanisms. In $CeRu_2Si_2$, critical ferromagnetic fluctuations [9, 29, 30] (accompanied by a Fermi surface Lifshitz transition [50]) drive the enhancement of A at H_m. Such critical ferromagnetic fluctuations probably play a role in $CeRh_2Si_2$ at H_m too. However, in sole magnetic-fluctuations frame there is no obvious reason why the enhancement should be so much larger at H_m than at H_c. The relatively 'low' value of the A coefficient extracted here indicates a moderate effective mass in $CeRh_2Si_2$. Under pressure, a decrease of the Kadowaki-Woods ratio A/γ^2 [51] and a reduction of the Ising character of the system [52] indicate the progressive recovery of the $N = 6$ degeneracy of the $J = 5/2$ multiplet, which could result from a Kondo temperature higher than the crystal-field energy scale [53], due to the proximity to a valence transition [54] (see also [55]). This picture is supported by the moderate and almost pressure-independent Sommerfeld coefficient $\gamma \simeq 80$ mJ/mol/K^2 in the high-pressure CPM regime (at zero magnetic field) [56], where a low-temperature Grüneisen parameter $\Gamma \simeq 7$, i.e., much smaller than in typical heavy-fermion paramagnets (cf. $CeRu_2Si_2$ where $\Gamma \simeq 200$ [57]), can also be extracted [58]. An open question is the evolution of the Fermi surface under pressure combined with magnetic field, i.e., through H_c and H_m at pressures close to p_x and p_c. At ambient pressure, the Fermi surface established experimentally in the AF phase agrees well with LDA+U band calculations [51, 59]. On crossing p_c, clear marks of Fermi surface change have been established, but a debate remains on the validity of its description by LDA, LDA+U, or some more sophisticated band calculation. Unfortunately, the Fermi surface of the PPM regime in fields above H_c has only be detected by the emergence of a single frequency [60]. New attempts to study the Fermi surface, but also valence, under combined pressure and magnetic field, allowing to access the PPM regime in magnetic fields higher than H_c and H_m, are now requested.

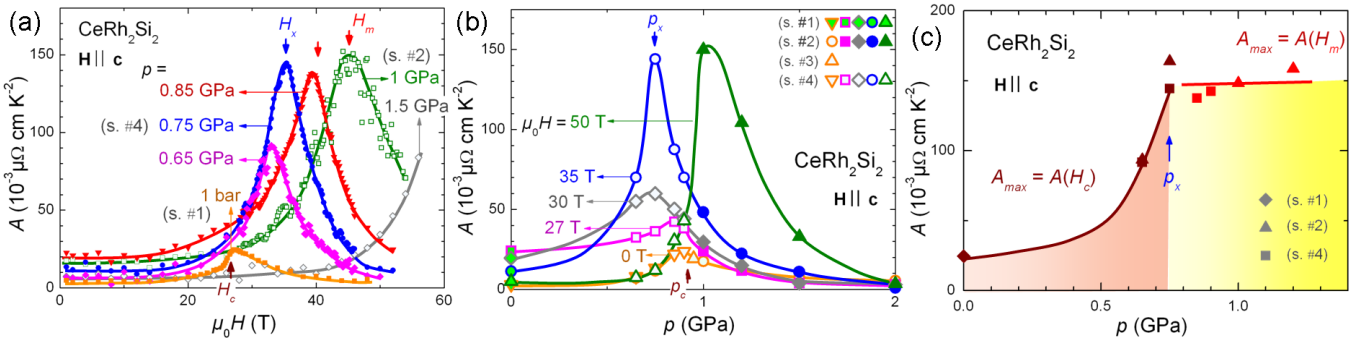

FIG. 7. Evolution of the Fermi liquid coefficient A as function of magnetic field and pressure. (a) A versus H, in magnetic fields up to 55 T, at different pressures. (b) A versus p, in pressures up to 2GPa, at different magnetic fields. (c) Pressure-dependence of A_{max} ($= A(H_c)$ for $p < p_x$ and $A(H_m)$ for $p > p_x$.

VI. CONCLUSION

The 3D phase diagram of $CeRh_2Si_2$, as well as the pressure- and magnetic-field-variations of its effective mass, confirm the importance of studying over a large temperature window the effects of pressure and magnetic field on quantum critical phenomena. The need to consider the high-temperature properties, such as the onset of antiferromagnetism and correlated paramagnetism, and their intimate relationship with the quantum properties, has been highlighted.

Thanks to a systematic tuning of a 3D phase diagram under combined pressure and magnetic field, we have determined the temperature and pressure dependences of the critical and pseudo-metamagnetic fields H_c and H_m, respectively. In particular, our study permitted to show:

1. that a low-temperature decoupling of H_c and H_m occurs in a narrow pressure range in the vicinity of the critical pressure p_c (at pressures $p_x < p < p_c$),

2. that this low-temperature decoupling of H_c and H_m results from a strong high-temperature decoupling of T_N and T_χ^{max},

3. that the decoupling of H_c and H_m can also occur in a limited temperature range when T_N and T_χ^{max} are not sufficiently decoupled (at pressures $p < p_x$).

A significant enhancement of the Fermi liquid coefficient A has also been observed at the critical point ($p_x = 0.75$ GPa, $\mu_0 H_x = 35$ T), which delimits the three low-temperature states (AF phase, CPM and PPM regimes), and on the critical line H_m, which separates the CPM and PPM regimes. From a sole magnetic-fluctuations picture, it is difficult to understand why the enhancement of A is much larger at H_m than at H_c. Additional effects, like changes of the Fermi surface, valence, and/or magnetic anisotropy, might also play a role in the critical enhancements of A. To go beyond the present study and understand the evolution of quantum criticality in the (p,H) phase diagram, further experiments (e.g., on magnetic fluctuations, valence, Fermi surface etc.) on $CeRh_2Si_2$, as well as new theoretical descriptions, are needed.

More generally, the combination of extreme conditions of intense magnetic field and high pressure constitutes a goldmine of novel phenomena in a large variety of strongly-correlated-electron systems. As in heavy-fermion systems, a decoupling of the long-range magnetic ordering and the maximum of the magnetic susceptibility is also observed in low-dimensional quantum magnets [61] and in high-temperature cuprate superconductors [62, 63]. Studying the evolution of this decoupling under combined pressure and magnetic field will shed new light on the quantum critical properties of these systems. In the region of optimal doping of cuprate superconductors, where several electronic energy scales fall drastically [63], it will be pertinent to test whether, and if so how, the quantum critical properties could be affected by intense magnetic fields.

ACKNOWLEDGEMENTS

We acknowledge J. Béard and M. Nardone for useful discussions. This work has been partly funded by the French ANR contract PRINCESS and the CEFIPRA project 4906 ExtremeSpinLadder.

APPENDIX

Fig. 8 presents how the different critical and crossover fields have been defined here. Fig. 8 (a) shows that, at ambient pressure (data from [27]), H_c is characterized by a step at low temperature, which progressively transforms into a maximum and then a kink at higher temperature, in the magnetoresistivity data. At temperatures above $T^* \simeq 30$ K and below $T_N(H = 0) = 36$ K, a broad maximum at a field ascribed to the pseudo-metamagnetic field H_m is decoupled from the kink at the critical field H_c. The different anomalies observed the resistivity at ambient pressure are summarized in the magnetic-field - temperature phase diagram in Fig. 8 (f). Fig. 8(b-e) show the magnetoresistivity obtained here on sample ♯2 at pressures from 0.65 to 1.2 GPa. At low temperature, the anomalies at H_c and H_m under pressure are broadened, in comparison with that at H_c at ambient pressure, presumably because of pressure inhomogeneities in the cells. In the light of other heavy-fermion paramagnets studies (see Ref. [15]) and for continuity in the data analysis, H_m has been defined at low temperature at the mid of a step in the resistivity, and at high temperature at the maximum of the resistivity. The magnetic-field - temperature phase diagrams obtained under pressure are plotted in Fig. 8 (g-j). They indicate that the correlated paramagnetic regime is progressively stabilized under pressure, extending from a narrow high-temperature region at ambient pressure to a large region down to the lowest temperature under pressures higher than $p_c \simeq 1$ GPa.

Figs. 9 (a-b) show the magnetoresistivity versus magnetic field data obtained at similar pressures of 1 and 0.95 GPa on samples ♯2 and ♯3, respectively, for a large set of temperatures from 2.1 to 100 K. This comparison emphasizes the very similar anomalies at H_m and H_{pol} observed in the magnetoresistivity of two samples of very different residual resistivity ratios (of $\simeq 40$ for sample ♯2 and $\simeq 145$ for sample ♯3), indicating that these anomalies are not controlled by an orbital effect, i.e., the field-induced cyclotron motion of the conduction electrons, and result from the magnetic properties of the system.

For all data, the fit by a T^2 law of the magnetoresistivity has been made in a temperature window from 1.5 to 10 K, the temperature having been corrected as de-

scribed in [42]. Fig. 10 (a-b) shows the T^2 variation of the resistivity extracted at $p = 0.9$ GPa on sample ♯4 using cell "2", for different fields up to 52 T, which indicates a significant enhancement of the quadratic coefficient A at 40 T. Fig. 10 (c-f) shows, in an extended temperature scale, the T^2 variation of the resistivity extracted for different values of the magnetic field, at $p = 1$ bar, 0.65 GPa, 0.85 GPa, and 1.2 GPa, indicating the departure from the low-temperature T^2 behavior at a temperature T^* estimated to $\simeq 8 - 10$ K at H_c and H_m, and to $\simeq 15$ K at magnetic fields far from H_c and H_m.

Fig. 11 (a) shows a comparison of the field-dependence (at ambient pressure) and the pressure-dependence (at zero-field) of the coefficient A extracted here for samples ♯1, ♯2, ♯3, and ♯4, confirming the similar enhancements of A up to $\simeq 25\ 10^{-3}\ \mu\Omega$cm K^{-2} observed at ($H_c$, $p = 1$bar) and ($H = 0$, p_c) reported previously [27, 46].

[1] J. A. Hertz, Phys. Rev. B **14**, 1165 (1976).
[2] T. Valla, A. V. Fedorov, P. D. Johnson, B. O. Wells, S. L. Hulbert, Q. Li, G. D. Gu, and N. Koshizuka, Science **285**, 2110 (1999).
[3] T. Shibauchi, A. Carrington, and Y. Matsuda, Annu. Rev. Condens. Matter Phys. **5**, 113 (2014).
[4] W. Knafo, S. Raymond, P. Lejay, and J. Flouquet, Nat. Phys. **5**, 753 (2009).
[5] R. Coldea, D. A. Tennant, E. M. Wheeler, E. Wawrzynska, D. Prabhakaran, M. Telling, K. Habicht, P. Smeibidl, and K. Kiefer, Science **327**, 177 (2010).
[6] P. Merchant, B. Normand, K. W. Kraemer, M. Boehm, D. F. McMorrow, and C. Rueegg, Nat. Phys. **10**, 373 (2014).
[7] G. R. Stewart, Rev. Mod. Phys. **73**, 797 (2001).
[8] R. A. Cooper, Y. Wang, B. Vignolle, O. J. Lipscombe, S. M. Hayden, Y. Tanabe, T. Adachi, Y. Koike, M. Nohara, H. Takagi, C. Proust, and N. E. Hussey, Science **323**, 603 (2009).
[9] D. Aoki, W. Knafo, and I. Sheikin, C. R. Physique **14**, 53 (2013).
[10] R. Settai, T. Takeuchi, and Y. Ōnuki, Journal of the Physical Society of Japan **76**, 051003 (2007).
[11] P. A. Lee, T. M. Rice, J. W. Serene, L. J. Sham, and J. W. Wilkins, Comment. Cond. Mat. Phys. **12**, 99 (1986).
[12] M. Ohashi, G. Oomi, S. Koiwai, M. Hedo, and Y. Uwatoko, Phys. Rev. B **68**, 144428 (2003).
[13] G. W. Scheerer, W. Knafo, D. Aoki, G. Ballon, A. Mari, D. Vignolles, and J. Flouquet, Phys. Rev. B **85**, 094402 (2012).
[14] N. Tsujii, H. Kontani, and K. Yoshimura, Phys. Rev. Lett. **94**, 057201 (2005).
[15] R. Daou, C. Bergemann, and S. R. Julian, Phys. Rev. Lett. **96**, 026401 (2006).
[16] R. A. Fisher, C. Marcenat, N. E. Phillips, P. Haen, F. Lapierre, P. Lejay, J. Flouquet, and J. Voiron, Journal of Low Temperature Physics **84**, 49 (1991).
[17] P. Gegenwart, Q. Si, and F. Steglich, Nat. Phys. **4**, 186 (2008).
[18] J. Flouquet, Prog. Low Temp. Phys. **15**, 139 (2005).
[19] H. v. Löhneysen, A. Rosch, M. Vojta, and P. Wölfle, Rev. Mod. Phys. **79**, 1015 (2007).
[20] C. Pfleiderer, Rev. Mod. Phys. **81**, 1551 (2009).
[21] S. Friedemann, T. Westerkamp, M. Brando, N. Oeschler, S. Wirth, P. Gegenwart, C. Krellner, C. Geibel, and F. Steglich, Nat. Phys. **5**, 465 (2009).
[22] A spin-flop transition corresponds to the sudden alignment of the AF moments perpendicular to the magnetic field and is accompanied by a step-like variation of the magnetization.
[23] K. Grube, W. Knafo, S. Drobnik, P. Adelmann, T. Wolf, C. Meingast, and H. Lhneysen, Journal of Magnetism and Magnetic Materials **310**, 354 (2007).
[24] W. Knafo, C. Meingast, K. Grube, S. Drobnik, P. Popovich, P. Schweiss, P. Adelmann, T. Wolf, and H. v. Löhneysen, Phys. Rev. Lett. **99**, 137206 (2007).
[25] E. Stryjewski and N. Giordano, Adv. Phys. **26**, 487650 (1977).
[26] R. Settai, A. Misawa, S. Araki, M. Kosaki, K. Sugiyama, T. Takeuchi, K. Kindo, Y. Haga, E. Yamamoto, and Y. Ōnuki, Prog. Low Temp. Phys. **66**, 2260 (1997).
[27] W. Knafo, D. Aoki, D. Vignolles, B. Vignolle, Y. Klein, C. Jaudet, A. Villaume, C. Proust, and J. Flouquet, Phys. Rev. B **81**, 094403 (2010).
[28] By tradition in the heavy-fermion community, the metamagnetic transition at the border of antiferromagnetism is usually noted H_c, while the pseudo-metamagnetic crossover at the border of correlated paramagnetism is usually noted H_m.
[29] J. Rossat-Mignod, L. Regnault, J. Jacoud, C. Vettier, P. Lejay, J. Flouquet, E. Walker, D. Jaccard, and A. Amato, J. Magn. Magn. Mater. **76-77**, 376 (1988).
[30] J. Flouquet, Y. Haga, P. Haen, D. Braithwaite, G. Knebel, S. Raymond, and S. Kambe, J. Magn. Magn. Mater. **272-276**, 27 (2004).
[31] B. Grier, J. Lawrence, V. Murgai, and R. Parks, Phys. Rev. B **29**, 2664 (1984).
[32] S. Kawarazaki, M. Sato, Y. Miyako, N. Chigusa, K. Watanabe, N. Metoki, Y. Koike, and M. Nishi, Phys. Rev. B **61**, 4167 (2000).
[33] T. Muramatsu, S. Eda, T. Kobayashi, M. Eremets, K. Amaya, S. Araki, R. Settai, and Y. Ōnuki, Physica B **259–261**, 61 (1999).
[34] R. Movshovich, T. Graf, D. Mandrus, J. D. Thompson, J. L. Smith, and Z. Fisk, Phys. Rev. B **53**, 8241 (1996).
[35] S. Araki, M. Nakashima, R. Settai, T. C. Kobayashi, and Y. Ōnuki, Journal of Physics: Condensed Matter **14**, L377 (2002).
[36] H. Abe, H. Suzuki, H. Kitazawa, T. Matsumo, and G. Kido, Journal of the Physical Society of Japan **66**, 2525 (1997).
[37] T. Hamamoto, K. Kindo, T. Kobayashi, Y. Uwatoko, S. Araki, R. Settai, and Y. Ōnuki, Physica B: Condensed Matter **281282**, 64 (2000).
[38] G. Knebel, J. Buhot, D. Aoki, G. Lapertot, S. Raymond, E. Ressouche, and J. Flouquet, J. Phys. Soc. Jpn. **80**, SA001 (2011).
[39] S. Zaum, K. Grube, R. Schfer, E. Bauer, J. Thompson, and H. v. Lhneysen, Phys. Rev. Lett. **106**, 087003 (2011).

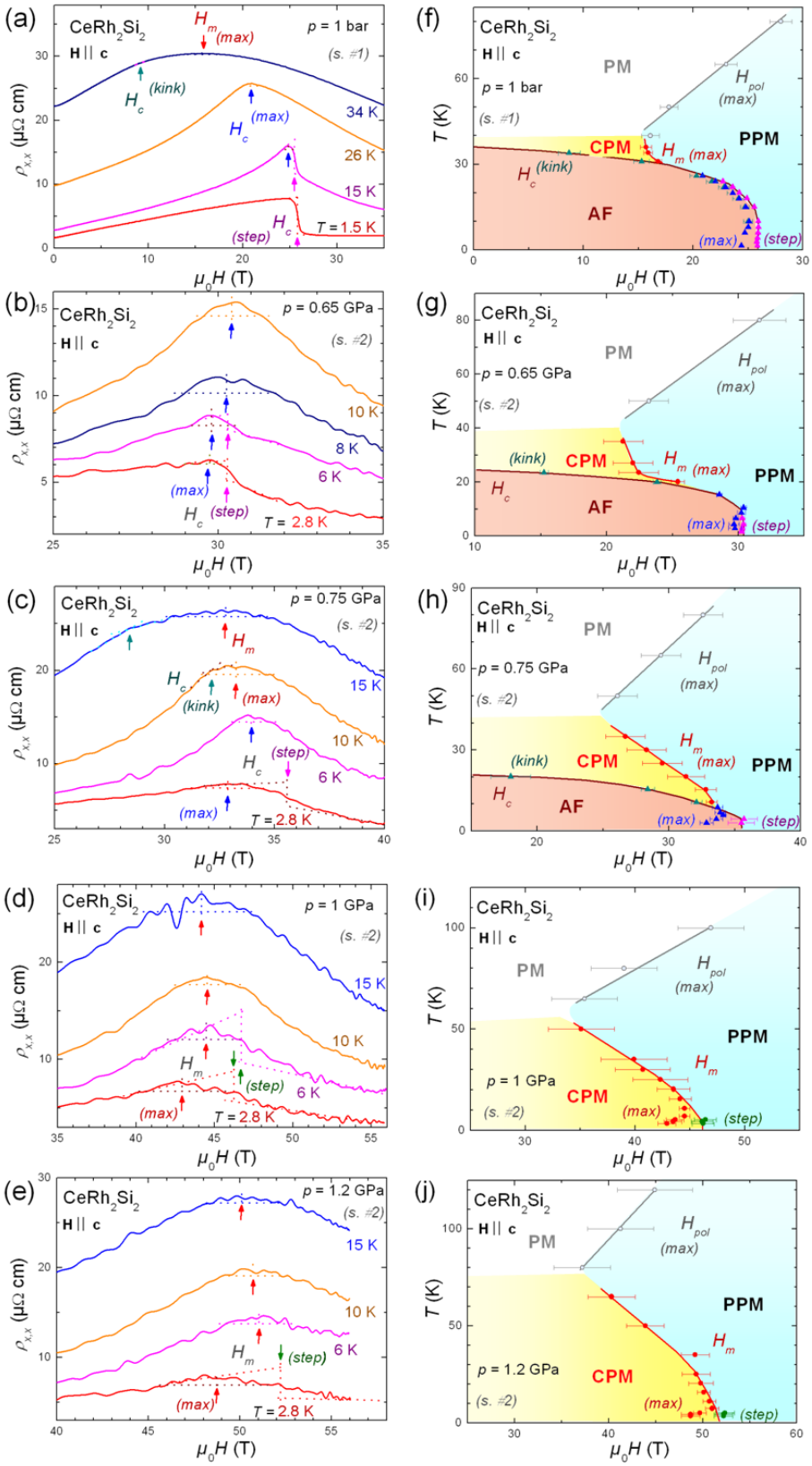

FIG. 8. Definition of the transitions and crossovers in the magnetoresistivity and phase diagrams extracted at different pressures. (a-e) Magnetoresistivity of sample ♯1 at ambient pressure, and of sample ♯2 at pressures from 0.65 to 1.2 GPa, under pulsed magnetic fields up to 56 T, at various temperatures from 1.5 to 34 K, and (f-j). corresponding magnetic-field - temperature phase diagrams obtained at constant pressures.

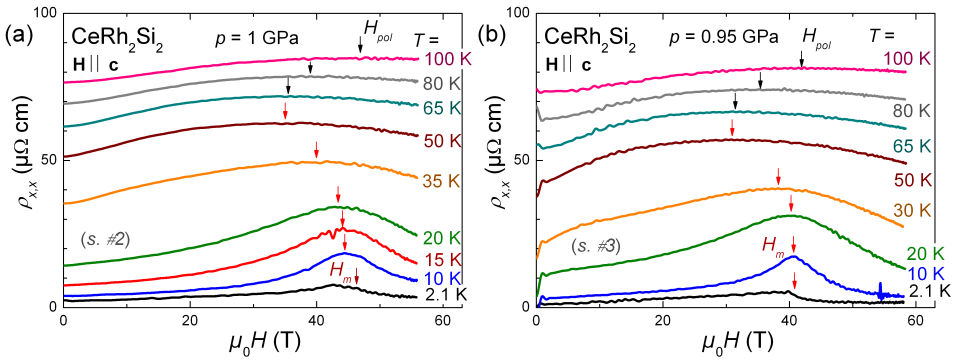

FIG. 9. Magnetoresistivity (a) of sample ♯2 at $p = 1$ GPa and (b) of sample ♯3 at $p = 0.95$ GPa at various temperatures from 2.1 to 100 K.

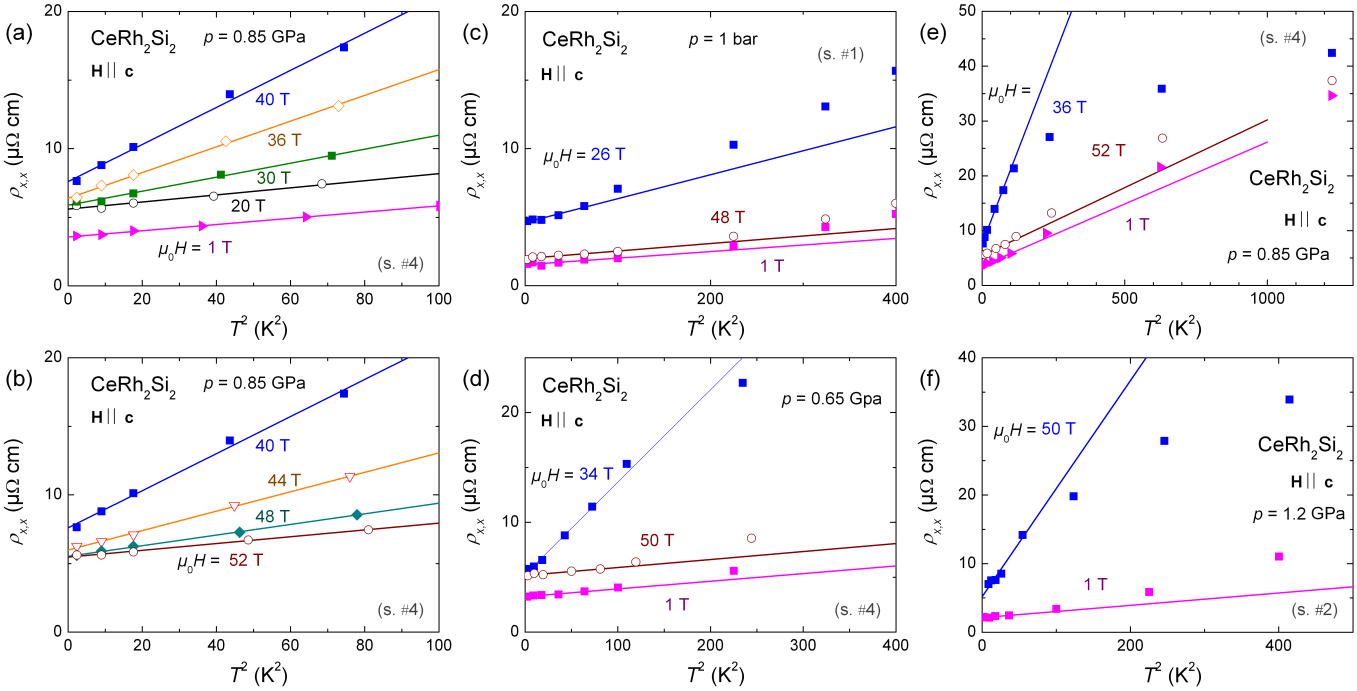

FIG. 10. (a-b) Resistivity versus T^2 of sample ♯4 at $p = 0.9$ GPa, for different fields up to 52 T. Resistivity versus T^2, in extended temperature scales, of (c) sample ♯1 at $p = 1$ bar, (d-e) sample ♯4 at $p = 0.65$ and 0.85 GPa, and (f) ♯2 at $p = 1.2$ GPa, for selections of magnetic field values from 1 to 52 T. The lines correspond to the fit to the data by a T^2 law.

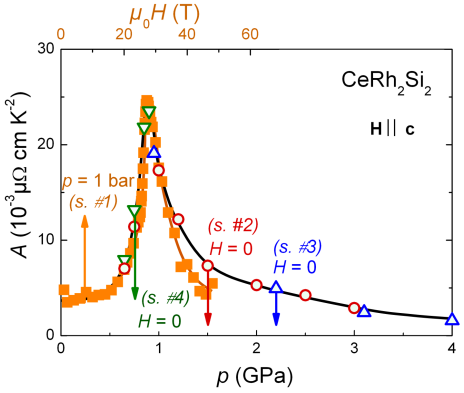

FIG. 11. Magnetic-field- and pressure-dependence of the quadratic coefficient A of the magnetoresistivity $\rho_{x,x}$ of $CeRh_2Si_2$ in $\mathbf{H} \parallel \mathbf{c}$. (a) Comparison of A versus H at $p = 1$ bar (sample ♯1) and A versus p at $H = 0$ (samples ♯2, ♯3, ♯4).

[40] K. Matsubayashi, T. Hirayama, T. Yamashita, S. Ohara, N. Kawamura, M. Mizumaki, N. Ishimatsu, S. Watanabe, K. Kitagawa, and Y. Uwatoko, Phys. Rev. Lett. **114**, 086401 (2015).

[41] M. Ohashi, F. Honda, T. Eto, S. Kaji, I. Minamitake, G. Oomi, S. Koiwai, and Y. Uwatoko, Physica B: Condensed Matter **312-313**, 443 (2002).

[42] D. Braithwaite, W. Knafo, R. Settai, D. Aoki, S. Kurahashi, and J. Flouquet, Review of Scientific Instruments **87**, 023907 (2016).

[43] R. Settai, W. Knafo, D. Braithwaite, S. Kurahashi, D. Aoki, and J. Flouquet, Review of High Pressure Science and Technology / Koatsuryoku No Kagaku To Gijutsu **25**, 325 (2015).

[44] See Refs. [13, 64], where a sample dependence of the orbital contribution to the high-field electrical resistivity, resulting from the cyclotron motion of conduction electrons, was evidenced in the heavy-fermion paramagnet URu_2Si_2.

[45] Y. Ōnuki, R. Settai, K. Sugiyama, T. Takeuchi, T. C. Kobayashi, Y. Haga, and E. Yamamoto, Journal of the Physical Society of Japan **73**, 769 (2004).

[46] J. Flouquet, D. Aoki, W. Knafo, G. Knebel, T. D. Matsuda, S. Raymond, C. Proust, C. Paulsen, and P. Haen, Journal of Low Temperature Physics **161**, 83 (2010).

[47] D. Aoki, C. Paulsen, H. Kotegawa, F. Hardy, C. Meingast, P. Haen, M. Boukahil, W. Knafo, E. Ressouche, S. Raymond, and J. Flouquet, Journal of the Physical Society of Japan **81**, 034711 (2012).

[48] P. Haen, F. Lapierre, J. Voiron, and J. Fouquet, J. Phys. Soc. Jpn. (Suppl. B) **65**, 27 (1996).

[49] D. Aoki, C. Paulsen, T. D. Matsuda, L. Malone, G. Knebel, P. Haen, P. Lejay, R. Settai, Y. nuki, and J. Flouquet, Journal of the Physical Society of Japan **80**, 053702 (2011).

[50] A. Pourret, D. Aoki, M. Boukahil, J.-P. Brison, W. Knafo, G. Knebel, S. Raymond, M. Taupin, Y. nuki, and J. Flouquet, Journal of the Physical Society of Japan **83**, 061002 (2014).

[51] A. Palacio Morales, A. Pourret, G. Seyfarth, M.-T. Suzuki, D. Braithwaite, G. Knebel, D. Aoki, and J. Flouquet, Phys. Rev. B **91**, 245129 (2015).

[52] H. Mori, N. Takeshita, N. Môri, and Y. Uwatoko, Physica B: Condensed Matter **259-261**, 58 (1999).

[53] K. Hanzawa, K. Yamada, and K. Yosida, J. Magn. Magn. Mater. **47-48**, 357 (1985).

[54] S. Watanabe and K. Miyake, Journal of Physics: Condensed Matter **23**, 094217 (2011).

[55] Y. H. Matsuda, J.-L. Her, S. Michimura, T. Inami, T. Ebihara, and H. Amitsuka, JPS Conf. Proc. **3**, 011044 (2014).

[56] T. Graf, J. D. Thompson, M. F. Hundley, R. Movshovich, Z. Fisk, D. Mandrus, R. A. Fisher, and N. E. Phillips, Phys. Rev. Lett. **78**, 3769 (1997).

[57] A. Lacerda, A. de Visser, P. Haen, P. Lejay, and J. Flouquet, Phys. Rev. B **40**, 8759 (1989).

[58] The Grüneisen parameter $\Gamma = 7$ is calculated in the pressure range $p > p_c$ following $\Gamma = \partial\gamma/\partial p/(\gamma\kappa)$, where $\partial\gamma/\partial p$ is extracted from [56] and the compressibility coefficient $\kappa = 0.74$ Mbar^{-1} is extracted from [12].

[59] S. Araki, R. Settai, T. C. Kobayashi, H. Harima, and Y. Ōnuki, Phys. Rev. B **64**, 224417 (2001).

[60] I. Sheikin, (unpublished).

[61] *Magnetic properties of layered transition metal compounds* (Kluwer Academic Publishers, Dordrecht / Boston / London, Edited by L.J. De Jongh, 1990).

[62] D. C. Johnston, Phys. Rev. Lett. **62**, 957 (1989).

[63] D. Pines, The Journal of Physical Chemistry B **117**, 13145 (2013).

[64] G. W. Scheerer, W. Knafo, D. Aoki, M. Nardone, A. Zitouni, J. Béard, J. Billette, J. Barata, C. Jaudet, M. Suleiman, P. Frings, L. Drigo, A. Audouard, T. D. Matsuda, A. Pourret, G. Knebel, and J. Flouquet, Phys. Rev. B **89**, 165107 (2014).